A unifying model for non-adiabatic coupling at metallic surfaces beyond the local harmonic approximation: From vibrational relaxation to scanning tunneling microscopy

Jean Christophe Tremblay

Citation: The Journal of Chemical Physics **138**, 244106 (2013); doi: 10.1063/1.4811150
View online: http://dx.doi.org/10.1063/1.4811150
View Table of Contents: http://scitation.aip.org/content/aip/journal/jcp/138/24?ver=pdfcov
Published by the AIP Publishing

A unifying model for non-adiabatic coupling at metallic surfaces beyond the local harmonic approximation: From vibrational relaxation to scanning tunneling microscopy

Jean Christophe Tremblay[a)]
Institute for Chemistry and Biochemistry, Freie Universität Berlin, Takustr. 3, D-14195 Berlin, Germany

(Received 12 April 2013; accepted 31 May 2013; published online 26 June 2013)

A model for treating excitation and relaxation of adsorbates at metallic surfaces induced by non-adiabatic coupling is developed. The derivation is based on the concept of resonant electron transfer, where the adsorbate serves as a molecular bridge for the inelastic transition between an electron source and a sink. In this picture, energy relaxation and scanning tunneling microscopy (STM) at metallic surfaces are treated on an equal footing as a quasi-thermal process. The model goes beyond the local harmonic approximation and allows for an unbiased description of floppy systems with multiple potential wells. Further, the limitation of the product ansatz for the vibronic wave function to include the position-dependence of the non-adiabatic couplings is avoided by explicitly enforcing detailed balance. The theory is applied to the excitation of hydrogen on palladium, which has multiple local potential minima connected by low energy barriers. The main aspects investigated are the lifetimes of adsorbate vibrations in different adsorption sites, as well as the dependence of the excitation, response, and transfer rates on an applied potential bias. The excitation and relaxation simulations reveal intricate population dynamics that depart significantly from the simplistic tunneling model in a truncated harmonic potential. In particular, the population decay from an initially occupied local minimum induced by the contact with an STM tip is found to be better described by a double exponential. The two rates are interpreted as a response to the system perturbation and a transfer rate following the perturbation. The transfer rate is found to obey a power law, as was the case in previous experimental and theoretical work. © *2013 AIP Publishing LLC*. [http://dx.doi.org/10.1063/1.4811150]

I. INTRODUCTION

Non-adiabatic effects at metallic surfaces have attracted much attention over the years. Evidences of electron-hole pair coupling mechanism include asymmetric line broadening in spectroscopy,[1–5] energy-loss upon recombinative desorption from, adsorption at, and absorption in metallic substrates,[6–21] and vibrational (de)-excitation of scattered molecules,[22–24] to name but a few. Many theoretical approaches have been developed to understand surface non-adiabaticity in the weak coupling regime.[25–37] Most of them rely on the harmonic approximation for the nuclear modes, while assuming that non-adiabatic couplings can be computed locally or that they are somehow independent of the adsorbate position. These constraints are not met for most molecule-surface systems, where multiple minima are connected by low-energy barriers along large amplitude diffusion coordinates. Only recently were these limitations addressed adequately,[38–40] where the adsorbate was embedded in an electron gas of variable density to mimic the position-dependence of the non-adiabatic coupling. In the model, numerical integration of the gradient operator was used to ensure proper treatment of anharmonicity.

The development of scanning tunneling microscopy (STM) in the early 1980s opened a whole new range of possibilities in surface science, in particular, the ability to manipulate individual atoms and molecules in the vicinity of a surface. The potential of this new method for the practical implementation of molecular switches was quickly recognized and exploited, as exemplified by the now famous Xe/Ni switch of Eigler *et al.*[41] Most of the theoretical understanding of the mechanisms at work in an STM is based on the Bardeen transfer Hamiltonian,[42,43] where the STM-to-surface electron transfer is mediated by a resonance state of the adsorbate. This model also allows to quantify the inelastic contributions to the current, which induce vibrational transitions in the adsorbate.[44–46] It was proposed independently by Walkup, Newns, and Avouris[47,48] and by Gao, Persson, and Lundqvist[49–52] that vibrational heating is responsible for the switching in the aforementioned system. In this case, energy is transferred from the electrons impinging from the STM tip to the adsorbate vibrations. In particular, in the latter work,[52] a clear connection between non-adiabatic coupling at metallic surfaces and STM-induced vibrational excitations was made. It was shown using first-order time-dependent perturbation theory that, in metallic environments, the heating rate is proportional to the product of the density of states of the STM and of the substrate, projected on the adsorbate resonance. Further, the model shows that the rates scale linearly with the potential bias of the STM tip and that they are directly proportional to the relaxation rate induced by electron-hole pair coupling. Many of the experimental features, such as the power law scaling of the atomic transfer rate, are well reproduced by

a)Electronic mail: jc.tremblay@fu-berlin.de

the theory, whereas the observed asymmetry of the rates with respect to the sign of the potential bias could be incorporated naturally in the model by modifying the molecule-surface interaction potential.

For all its qualities, the approach unfortunately relies on the local harmonic approximation, which will break down for anharmonic and floppy systems with multiple minima, as mentioned above. It is the main goal of the present work to develop a physically sound model that goes beyond these limitations while keeping its most attractive features. Since the position-dependent anharmonic rate model introduced recently[38–40] cannot be extended straightforwardly to treat STM-induced excitations, an alternative derivation is proposed. To avoid the pitfalls associated with the identification and the characterization of a single adsorbate resonance, the model of Gao *et al.*[49–52] is reinterpreted using source-bridge-sink terminology, where the source and sink density of states are projected on a physical bridge state located at the position of the adsorbate, hence allowing to recover the position-dependence of the non-adiabatic couplings.

In Sec. II, the electron-hole pair coupling mechanism at metallic surfaces is introduced and applied to the zero-current limit and for STM-induced non-adiabatic transitions. The model is applied to hydrogen in palladium in Sec. III. The implications of the model on the relaxation/excitation rates for the zero-current and STM-induced cases are discussed in Subsections III A and III B, respectively. Dynamical simulations are performed in Subsection III C. The findings are summarized in the conclusion, Sec. IV. Several mathematical aspects of the model are described in some detail in the Appendix.

II. ELECTRON-HOLE PAIR COUPLING MODEL

Let us start with the Hamiltonian of an adsorbate in the vicinity of a metallic surface. It can be written as a sum of electronic contributions from the metal, $\hat{H}_e$, and vibrational contributions from the adsorbate, $\hat{H}_v$, coupled via an operator $\hat{H}_{ev}$:

$$\hat{H} = \hat{H}_e \otimes \hat{I}_v + \hat{I}_e \otimes \hat{H}_v + \hat{H}_{ev}. \tag{1}$$

This Hamiltonian is different than the one used by Gao and co-workers[52] for similar systems, where they postulate that non-adiabatic coupling causes a linear energy shift of an electronic resonance located on the adsorbate. Here, we will consider more generally that non-adiabatic coupling is mediated by the kinetic energy operator of the nuclei, which for a single mode q of mass m_q reads

$$\hat{H}_{ev} = \frac{-\hbar^2}{2m_q}\frac{\partial^2}{\partial q^2}. \tag{2}$$

The non-adiabatic coupling between metal electrons and adsorbate vibrations induces electronic transitions in the metal. This approach has been followed by others as well.[53]

In Subsection A 1 of the Appendix, it is demonstrated how non-adiabatic transition rates can be computed using first-order perturbation theory beyond the local harmonic approximation. It is postulated that the electrons that mediate the non-adiabatic couplings transfer from a source to an electron sink via a bridge localized at the adsorbate. The following general expression,

$$\Gamma^{(q)}_{i\to j} \simeq \frac{2\pi\hbar}{m_q^2\omega_{ij}^2}\left\{\langle j|\epsilon'_a\rho^{source}(\epsilon_F)\frac{\partial}{\partial q}|i\rangle\right\}\left\{\langle i|\frac{\partial}{\partial q}\epsilon'_a\rho^{sink}(\epsilon_F)|j\rangle\right\} \times \int_0^{\hbar\omega_{ij}+eU} d\epsilon f_\beta(\epsilon_F-\epsilon)(1-f_\alpha(\epsilon_F-\epsilon+\hbar\omega_{ij})), \tag{3}$$

covers both the situations where the system is in contact with the tip of a STM and the zero-bias limit of the electron-hole pair coupling mechanism. These scenarios are depicted in Figure 1. Here, U is the potential bias of the STM tip, $\hbar\omega_{ij}$ is the energy difference between vibrational states $|i\rangle$ and $|j\rangle$, $\rho^s(\epsilon_F)$ is the density of electronic states of the source ($s = source$) or the sink ($s = sink$), and $f_{\alpha,\beta}$ are Fermi distributions for the initial and final electronic states. The term $\epsilon'_a = \langle a|\frac{\partial \hat{H}_e}{\partial q}|a\rangle$ is the variation of the electronic energy as a function of the nuclear coordinate q with associated mass m_q, projected on the adsorbate bridge $|a\rangle$. The dependence of ϵ'_a and $\rho^s(\epsilon_F)$ on the nuclear coordinates has been omitted here to simplify notation.

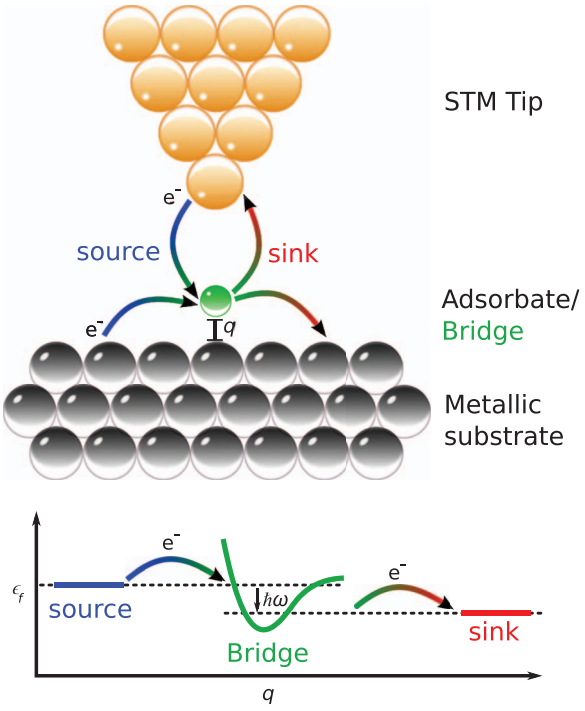

FIG. 1. Schematic representation of the non-adiabatic coupling of an adsorbate to a source (blue) and a sink (red) of density of states. The electrons are transferred either from a STM tip (orange) or a metallic substrate (grey) via a molecular bridge (green). The energy representation of the transfer is depicted in the bottom panel. An electron hops from the source to the bridge at a rate that depends on the position q of the adsorbate. Energy ($\hbar\omega$) is transferred from the electron to the anharmonic vibrations of the bridge, before the electron hops to the sink at lower energy.

It is important to recognize that there are no physical restrictions on the adsorbate bridge state. In particular, it is not required that the state is an eigenstate of the electronic Hamiltonian. It could be any linear combination of many overlapping resonances, for example. This is a consequence of the choice of projectors in Eqs. (A7) and (A8) to simplify

the evaluation of the non-adiabatic coupling elements. The delocalized electronic states of the system are projected on an effective electronic state $|a\rangle$ localized on the adsorbate. This so-called "bridge state" is a linear combination of all electronics eigenstates of the system, those labeled as belonging to the source and those to the sink (see Subsection A 1 of the Appendix for the mathematical development). The indirect coupling between the bridge state and the complementary space is neglected, which allows to rewrite the equation as a function of the projected density of states. The latter is assumed to remain constant on the energy range of the transitions, $\rho^s(\epsilon) \simeq \rho^s(\epsilon_F)$, a simplification that has also been used by others in similar context.[45,52,54]

In the zero-bias limit, the model can be shown to reduce to a form very similar to the recently published position-dependent anharmonic rate model for non-adiabatic coupling at metallic surfaces (see Subsection A 2 of the Appendix for more details):[38]

$$
\begin{aligned}
{}^{\mathrm{eh}}\Gamma^{(q)}_{i\to j} &\simeq \frac{\gamma^{(q)}}{\omega_{ij}}\left|\langle j|\mathbf{n}^{1/3}\frac{\partial}{\partial q}|i\rangle\right|^2 (1+B(\hbar\omega_{ij}));\\
{}^{\mathrm{eh}}\Gamma^{(q)}_{i\leftarrow j} &\simeq \frac{\gamma^{(q)}}{\omega_{ij}}\left|\langle j|\mathbf{n}^{1/3}\frac{\partial}{\partial q}|i\rangle\right|^2 B(\hbar\omega_{ij});
\end{aligned}
\qquad \text{where } \gamma^{(q)} = \left(\frac{2\hbar\Gamma^{(ref,q)}}{m_q \mathbf{n}^{2/3}_{(ref)}}\right). \tag{4}
$$

The adsorbate is embedded in a spherical jellium with a density $\mathbf{n}$ given by the electronic density of the metal surrounding the adsorbate impurity.[55] It mimics the dependence of the gradient of the electronic state (i.e., the non-adiabatic coupling strength) on the position and geometry of the adsorbate. The anharmonicity of the vibrational wave functions, $|i\rangle$, is included by integrating numerically the operator, $(\mathbf{n}^{1/3}\frac{\partial}{\partial q})$, over the full-dimensional vibrational wave functions. Although the gradient operator is unidimensional, both the embedding density and the initial and final vibrational states depend on all nuclear coordinates, and multi-dimensional numerical integration allows to recover potential intermode coupling.

An important difference with our previous model is that the energy-dependence of the transition rates due to electron-hole pair coupling is included explicitly here and found to be inversely proportional to the transition energy. This picture is physically satisfying since coupling between energy levels that lie energetically far apart is expected to be weak. Further, the temperature-dependence of the downward ${}^{\mathrm{eh}}\Gamma^{(q)}_{i\to j}$ and upward ${}^{\mathrm{eh}}\Gamma^{(q)}_{i\leftarrow j}$ transition rates is taken into account by the Bose-Einstein distribution, $B(\hbar\omega_{ij})$. As the temperature rises, both upward and downward rates tend to infinity and their ratio tends towards 1.

To determine the scaling constant $\gamma^{(q)}$, Eqs. (3) and (4) are taken to their local harmonic limit at T = 0 K for a geometry where this approximation holds. Resolving the perturbative expression (3) in the basis of one-electron Kohn-Sham states, $\left\{|\tilde{\alpha}\rangle, |\tilde{\beta}\rangle\right\}$, the transition rate for the fundamental transition can be computed as[45]

$$
\Gamma^{(ref,q)} = \frac{\pi}{m_q\omega_q}\sum_{\tilde{\alpha},\tilde{\beta}\mathbf{k}}\left|\langle\tilde{\alpha}\mathbf{k}|\left(\frac{\partial\hat{v}_{KS}}{\partial q}\right)\Big|_{ref}|\tilde{\beta}\mathbf{k}\rangle\right|^2 \times \delta(\varepsilon_{\tilde{\alpha},\mathbf{k}} - \varepsilon_{\tilde{\beta},\mathbf{k}} + \hbar\omega_q). \tag{5}
$$

Here, $\varepsilon_{n,\mathbf{k}}$ are band energies at a given point $\mathbf{k}$ in the Brillouin zone, associated with an occupied ($n = \tilde{\beta}$) or an empty ($n = \tilde{\alpha}$) band. The variation of the Kohn-Sham potential with respect to the qth coordinate at the reference geometry, $(\frac{\partial\hat{v}_{KS}}{\partial q})|_{ref}$, can be evaluated by finite differences. The scaling constant is obtained by matching both results, see Subsection A 2 of the Appendix for more detail.

At finite bias U, electrons are exchanged between the source and the sink, which have in general different densities of states in Eq. (3). The left and right panels of Figure 2 show an electron initially in a state of the STM tip or the metal, respectively, projected on the bridge represented by green gaussians. After losing the energy to the adsorbate vibrations, the electron proceeds to the sink (the metal or the STM tip, respectively) and the hole left behind decays in the source. The surface is considered grounded, i.e., the electron-hole pairs in the surface created by the electron transfer relax instantaneously. It is shown in Subsection A 3 of the Appendix that expression (3) can be reduced to the form,

$$
{}^{\mathrm{stm}}\Gamma^{(q)}_{i\to j} \simeq w_s\left(\frac{|eU|}{\hbar\omega_{ij}}\right)\left(\frac{\gamma^{(q)}}{\omega_{ij}}\right)\left|\langle j|\mathbf{n}^{1/3}\frac{\partial}{\partial q}|i\rangle\right|^2, \tag{6}
$$

where $\gamma^{(q)}$ is the same as for the relaxation rates, Eq. (4). A position-dependent, locally spherical embedding electron density proportional to the s-projected electron density of the metal is postulated throughout. The constant factor w_s gives the efficiency of the STM mechanism as compared to the non-adiabatic coupling at zero bias.

Note that, according to Eq. (6), the STM-induced non-adiabatic transition rates are symmetric with respect to the sign of the potential bias. As pointed out by Gao *et al.*,[52] the experimentally observed asymmetry of the transition rates with respect to the sign of the potential bias[56] is due to the distortion of the potential energy surface induced by the STM tip, which can affect the potential energy barriers. The distortion of the potential could be added to present model by

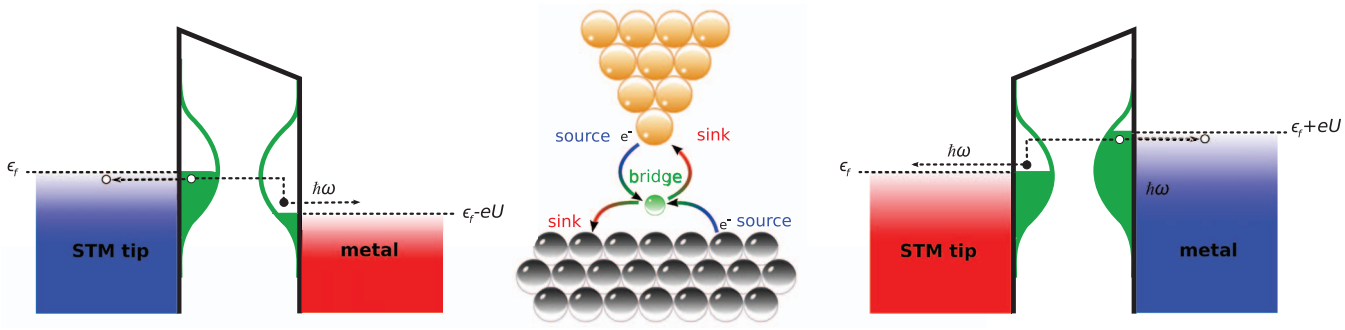

FIG. 2. The central panel depicts schematically the inelastic electron transfer from a STM tip (orange) to a metallic substrate (grey) via an adsorbate bridge (green), as well as the reverse process. The left panel shows the electron (black dot) leaving the bridge for the metal after having lost some energy to the adsorbate vibrations, while the hole left behind (white dot) decays to inside the STM tip. The right panel shows the reverse situation.

considering in Eq. (3) the position-dependent variation of the electronic Hamiltonian as a function of the applied bias,

$$\epsilon'_a \to \epsilon'_a(U) = \langle a|\frac{\partial \hat{H}_e(U)}{\partial q}|a\rangle = \langle a|\left(\frac{\partial \hat{H}_e(0)}{\partial q} - e\frac{\partial \Phi(U)}{\partial q}\right)|a\rangle, \quad (7)$$

where $\Phi(U)$ is the local electrostatic potential at the adsorbate position q. This modification is far from trivial, since the function $\Phi(U)$ is not exactly known, which would add an arbitrary source of error in the model. According to Gao and co-workers,[52] this contribution is small for similar systems. The usual simplifying assumption is to neglect the variation of $\Phi(U)$ as a function of the position on the surface altogether.[45,51–54,57,58]

Taking the ratio of Eq. (6) to the electron-hole pair transition rate, Eq. (4), the STM-induced rate expression becomes

$${}^{\rm stm}\Gamma^{(q)}_{i\to j} \simeq w_s\left(\frac{|eU|}{\hbar\omega_{ij}}\right)\gamma^q_{ij}, \quad (8)$$

where $\gamma^q_{ij} = {}^{\rm eh}\Gamma^{(q)}_{i\to j}(T=0)$. Reversibility is enforced explicitly by imposing that $\Gamma^{(q)}_{i\leftarrow j} = \Gamma^{(q)}_{i\to j}$. The final expression bears some similarities to equation (3) in the work of Blanco-Rey *et al.*,[53] provided the current-dependence is linearized as in their work. It compares also well to that of Gao and co-workers,[52] which reads in the present notation:

$${}^{\rm stm}\Gamma^{(q)}_{loc} \simeq \left(\frac{\Delta_{source}}{\Delta_{sink}}\right)\left(\frac{|eU|}{\hbar\omega_{10}}\right)\gamma^q_{loc}. \quad (9)$$

Here, γ^q_{loc} is the rate at zero bias for the $1\to 0$ transition in the local harmonic limit. As argued elsewhere,[52] reasonable estimates for the partial width of the source Δ_{source} and the sink Δ_{sink} can be obtained from experiment, which could then be used to define the constant w_s. Although losing the *ab initio* character of the model, it is deemed preferable to keep the constant w_s as a free parameter. Since its effect on the STM-induced rates is linear, it can be compensated in principle by a larger or smaller effective potential bias.

In the spirit of first order perturbation theory, the dipole contribution to the total rate could be simply added to the present model.[44,58,59] Because of the small magnitude of the STM-induced field at the surface and the efficient screening of the field by the electrons inside the metal, the former contribution is neglected altogether.[52] In the present work, the focus is on the non-adiabatic effects in metallic environments and vibration-phonon coupling is neglected as well. The total upward and downward transition rates thus read

$$\Gamma_{i\to j} = \sum_q\left(1 + B(\hbar\omega_{ij}) + w_s\left(\frac{|eU|}{\hbar\omega_{ij}}\right)\right)\gamma^q_{ij},$$
$$\Gamma_{i\leftarrow j} = \sum_q\left(B(\hbar\omega_{ij}) + w_s\left(\frac{|eU|}{\hbar\omega_{ij}}\right)\right)\gamma^q_{ij}. \quad (10)$$

III. APPLICATION TO H/Pd(111)

A. Relaxation rates

The vibrational dynamics of hydrogen on palladium is a good toy system to test the present model. The potential energy surface has multiple local minima connected by low-energy barriers and the system is thus strongly anharmonic and exhibits large amplitude motions. The details for the calculation of the 3D anharmonic vibrations on the potential energy surface of Ozawa *et al.*[60] (labeled ORNKAD after the authors) using a conventional variational procedure are given elsewhere.[38] The energies of the perpendicular (ν_z) and of the doubly degenerate parallel mode (ν_p) relative to the global ground state are reported in the last column of Table I. From harmonic calculations for a hydrogen atom in bulk palladium,[53] the *Z*-mode frequency in the bulk octahedral cavity is estimated as $\hbar\omega = 379$ hc/cm. The agreement with 1D calculations on a the ORNKAD potential following a relaxed energy path perpendicular to the surface is fair ($\hbar\omega = 466$ hc/cm), but comparison with the full 3D transition energy (633 hc/cm) is rather poor. This is due to the strong mixing of the harmonic modes. Nonetheless, the vibrational wave functions associated with both the bulk ground state and the first excited states are well localized in the octahedral cavity, in good agreement with previously published theoretical results.[53]

The inverse transition rate due to electron-hole pair coupling from the first perpendicular mode excited state ($|1, 0, f\rangle$) to the bulk ground state computed using Eq. (4)

TABLE I. Inverse downward transition rates computed using Eq. (4) for selected vibrational states of H/Pd(111). The states are labeled by their nodal structure perpendicular and along the surface, $|\nu_z, \nu_\rho; i\rangle$, in different local centers $i = \{f, h, s, b\}$. The transition energies in parentheses are expressed relative to the ground state in the local center.

Initial state		Final state				
State number	Assignment	$\|0, 0; f\rangle$	$\|0, 0; h\rangle$	$\|0, 0; s\rangle$	$\|0, 0; b\rangle$	E (hc/cm)
$\|1\rangle$	$\|0, 0; h\rangle$	*1.1 μs*	…	…	…	288.3
$\|2, 3\rangle$	$\|0, 1; f\rangle$	**470 fs**	208 ps	…	…	717.4
$\|4\rangle$	$\|1, 0; f\rangle$	**529 fs**	395 ps	…	…	922.4
$\|5, 6\rangle$	$\|0, 1; h\rangle$	87 ps	**515 fs**	…	…	928.2 (639.9)
$\|7\rangle$	$\|1, 0; h\rangle$	3.8 ps	1.5 ps	…	…	1117.7 (829.4)
$\|39\rangle$	$\|0, 0; s\rangle$	*29 μs*	*10 μs*	…	…	2540.5
$\|61\rangle$	$\|1, 0; s\rangle$	*189 μs*	*199 μs*	**466 fs**	…	3146.2 (605.7)
$\|63, 64\rangle$	$\|0, 1; s\rangle$	***>1 s***	***>1 s***	**477 fs**	…	3178.7 (638.2)
$\|68\rangle$	$\|0, 0; b\rangle$	*356 ns*	*52 ns*	*15 μs*	…	3217.6
$\|102, 103\rangle$	$\|0, 1; b\rangle$	***>1 s***	***>1 s***	***>1 s***	**435 fs**	3841.8 (624.2)
$\|104\rangle$	$\|1, 0; b\rangle$	***>1 s***	***>1 s***	***>1 s***	**419 fs**	3850.6 (633.0)

at 0 K is $\Gamma_{|1,0;f\rangle \to |0,0;f\rangle} = 529$ fs. The reference lifetime is calculated at the global ground state geometry, located at the fcc surface site, using Eq. (5). The perpendicular and parallel mode lifetimes are found to be equal within the uncertainty associated with this first principle model, as discussed elsewhere.[39] The reference lifetime for all modes is set equal to $1/\Gamma_{(ref)} = 393$ fs, consistent with the picture of an atom thwarted by electronic friction in a locally isotropic medium. This sub-picosecond order of magnitude also compares well with the scattering lifetime of an impurity moving in a free electron gas,[25–27,29–31,33] as well as with the experimentally measured line broadening in similar hydrogen-metal systems.[61–63]

Further inverse transition rates are also reported in Table I for selected states. These state-resolved lifetimes are shown in bold, underlined, bold-italics, italics, and italics-underlined according to their timescale for convenience. The bold and underlined rates will dominate the relaxation dynamics, whereas the bold-italics rates describe extremely weak transition probability (numerically zero). The lowest states localized at each center (fcc, hcp, subsurface, and bulk) also have very long lifetime, in the microsecond regime for the subsurface (italics) and in the nanosecond regime for the bulk (italics-underlined, italics). These states should remain stable on the timescale where dynamical events can be controlled at the surface. Note that the inverse transition rate of the reference state $|1, 0; f\rangle$ computed using Eq. (4) is longer than the reference value computed in the local harmonic approximation. The deviation points out at strong intermode coupling and anharmonic effects even at such low energies. Some remaining small discrepancies with our previous results come from the explicit inclusion of the energy dependence in the transition rate expression, which was previously neglected.[38,39]

B. STM-induced rates

It was shown recently that the STM-induced rates in the bulk are mediated by the *s*-electrons of the metal.[53] This finding can be used to get an estimate of the scaling constant in Eq. (8). Using Eq. (9), one can conclude that the scaling constant w_s is given by

$$w_s = \frac{\Delta_{source}}{\Delta_{sink}} = \frac{\rho^{source}(\epsilon_F)}{\rho^{sink}(\epsilon_F)}. \tag{11}$$

It is postulated in Sec. II that $\rho^{source}(\epsilon_F) \simeq w_s \rho^{sink}(\epsilon_F)$. A fitting choice is to compute the scaling constant w_s as the ratio of the *s*-projected density of states in the substrate to the total density of states, which allows to recover the *s*-wave electron propagation mechanism inside the bulk. This might introduce a small error at the surface, where the *p* and *d* orbitals of the STM tip should play a role in the injection process. As argued in Subsection A 3 of the Appendix, the locally spherical electron density surrounding the atomic impurity at any position will not be strongly affected by the presence of these orbitals, with the exception of the close vicinity of the STM tip.

To represent the Pd(111) surface, a 1 × 1 slab consisting of 6 layers of palladium (lattice constant: 3.98 Å) surmounted by a vacuum of 11.4 Å is used. The electron structure is calculated self-consistently using periodic density functional theory with scalar relativistic ultrasoft pseudopotentials[64] and the Perdew-Burke-Ernzerhof (PBE) functional,[65] as implemented in the Quantum Espresso package.[66] A 16 × 16 × 1 Monkhorst-Pack grid[67] with energy and charge density cutoffs of 50 and 500 Ry is used in all calculations, and the energy is converged to 10^{-7} Ry. Using these results, the calculated value of the STM scaling constant is $w_s \sim \frac{\rho_s(\epsilon_F)}{\rho_{tot}(\epsilon_F)} = 0.02$, which is in line with the value found by Gao and co-workers for xenon on nickel ($w_s = 0.07$).[52] The calculation is repeated with a hydrogen atom adsorbed at its minimal position on the surface for comparison. The ratio of *s*-projected density of states to the total density of states at the Fermi energy is found to remain unaffected. We argue that the value $w_s \sim 0.02$ should thus remain almost constant at every position of the adsorbate, inside and outside the surface. This assumption is reasonable considering the very small contribution of the hydrogen impurity to the total density of states. For larger adsorbates, this particularly convenient condition might not hold. Blanco-Rey and co-workers[53] find STM-induced

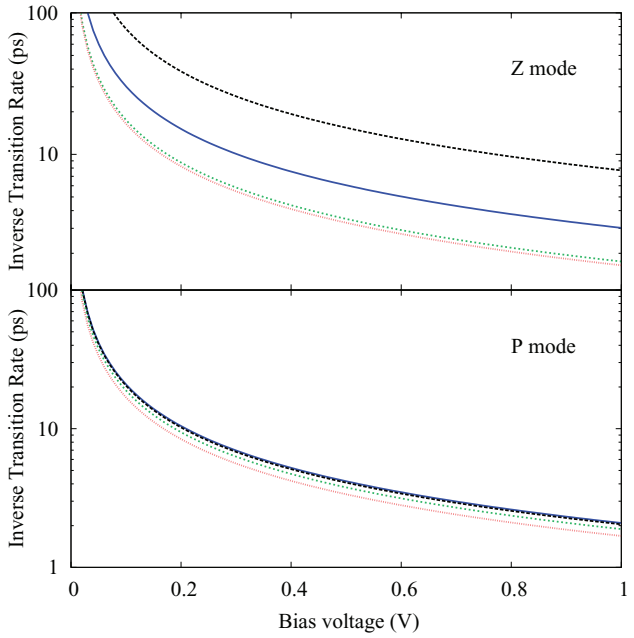

FIG. 3. Behavior of the STM-induced transition rates as a function of the potential bias, computed according to Eq. (8). The scaling factor is set to $w_s = 0.02$. (Top panel) Inverse rate (ps) for the perpendicular (Z) mode excitation from a given local minimum; fcc (dotted orange), hcp (dashed green), subsurface (solid blue), and bulk (long dashed black). (Bottom panel) Inverse rate (ps) for the parallel (P) mode excitation from a given local minimum; same colors as above.

transition rates on the order of a few GHz at bias voltage below 1 V (e.g., for $U = 1$ V, ${}^{\text{stm}}\Gamma^{(ref)} = 34.5$ GHz). This is much slower than the rates found using other first principle methods,[45] a discrepancy that could be attributed to the choice of pseudopotential.

Figure 3 shows the bias voltage dependence of the STM-induced rates for the perpendicular and parallel mode excitations from their local ground state. One can see that the rates associated with the perpendicular mode at the surface (fcc in red, hcp in green) are slower than that inside the metal (subsurface and bulk in blue and magenta, respectively). The parallel mode rates behave, on the other hand, very similarly at any given position. The lifetimes associated with the STM-induced excitation process are consistently shorter for the parallel mode, which means that lateral displacements might be easier to excite and to control using a STM tip. The inverse rates are found to be well above 1 ps for all transitions in the range of bias potentials depicted here due to the weak coupling efficiency with the STM tip ($w_s = 0.02$). Since the relaxation lifetimes at zero bias are much shorter (around 500 fs for the reported transitions), it also implies that any transient excited population would relax back at a faster rate than it could be excited, leading to poor transfer yields. This effect will also be exacerbated by including all other possible dissipation channels that have been made accessible by our treatment of anharmonic coupling and the position-dependence of the non-adiabatic couplings, Eq. (4). An example of such effect is given in Table I. The first excited state along Z located in the hcp minimum is seen to decay at a similar rate to both the fcc and hcp ground states. Intermode conversion is also observed at even lower energy, where the first excited state along Z located in the fcc (global) minimum relaxes within 1.4 ps to the parallel mode state – a mere factor of 3 slower than the dominant relaxation channel.

C. Dissipative dynamics

Since both mechanisms in the transition rates expression (10) are incoherent mechanisms, the STM-induced dynamics can be described by the Pauli master equation. The time-evolution of the population $P_n(t)$ of a given vibrational state $|n\rangle = |\nu_z, \nu_p; i\rangle$ obeys

$$\frac{\mathrm{d}P_n(t)}{\mathrm{d}t} = \sum_j (\Gamma_{j\to n} P_j(t) - \Gamma_{n\to j} P_n(t)). \qquad (12)$$

Note that the equation is valid in the Markovian limit, which means that the metallic environment reacts instantaneously to any change in the adsorbate dynamics and it has no memory of its interaction with the system. Contrary to other approaches invoking the local harmonic approximation, the rates of all transfer channels $\Gamma_{j\to n}$ are considered here. For the dynamics, the lowest-lying 821 states at energy below ~10 000 hc/cm are included. Although a clear progression along the perpendicular and parallel coordinates can be identified for the first few excited states, this simple picture falls quickly apart with increasing energy. This is due to the low diffusion barrier (~1250 hc/cm) and small energy difference between the fcc and hcp sites (~325 hc/cm), which induce strong mixing of the lateral modes.

To probe the dynamics, three different initial conditions are chosen: the fcc ground state $|0, 0; f\rangle$, the subsurface octahedral site $|0, 0; s\rangle$, and the bulk octahedral site $|0, 0; b\rangle$. Varying the bias voltage of the STM tip will affect the population transfer from the initial state to the other metastable sites. The above-threshold atom transfer is depicted schematically in Figure 4 for the coordinate perpendicular to the

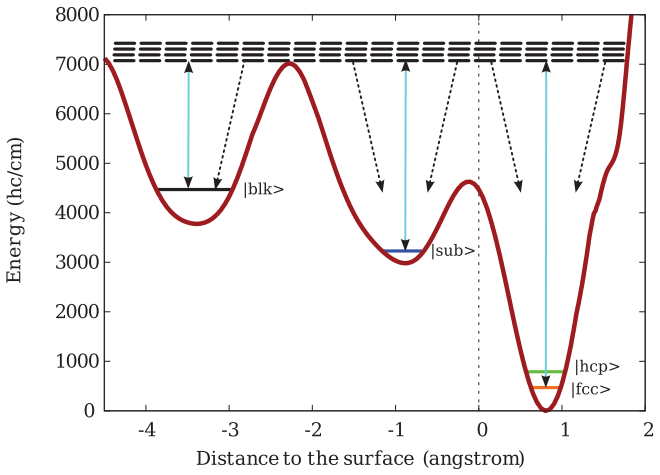

FIG. 4. One-dimensional schematic representation of the above-threshold excitation mechanism using a scanning tunneling microscope along the coordinate perpendicular to the surface. The system is initially prepared in either the fcc ground state (orange), the subsurface octahedral site (blue), or the bulk octahedral site (black). Non-adiabatic effects induced by the STM tip couple the initial states to delocalized states (horizontal dashed black lines) above the diffusion barriers, represented by cyan arrows. Upon relaxation, the system decays to either one of the three local minima (dashed arrows). The vertical dashed grey line denotes the position of the first surface layer.

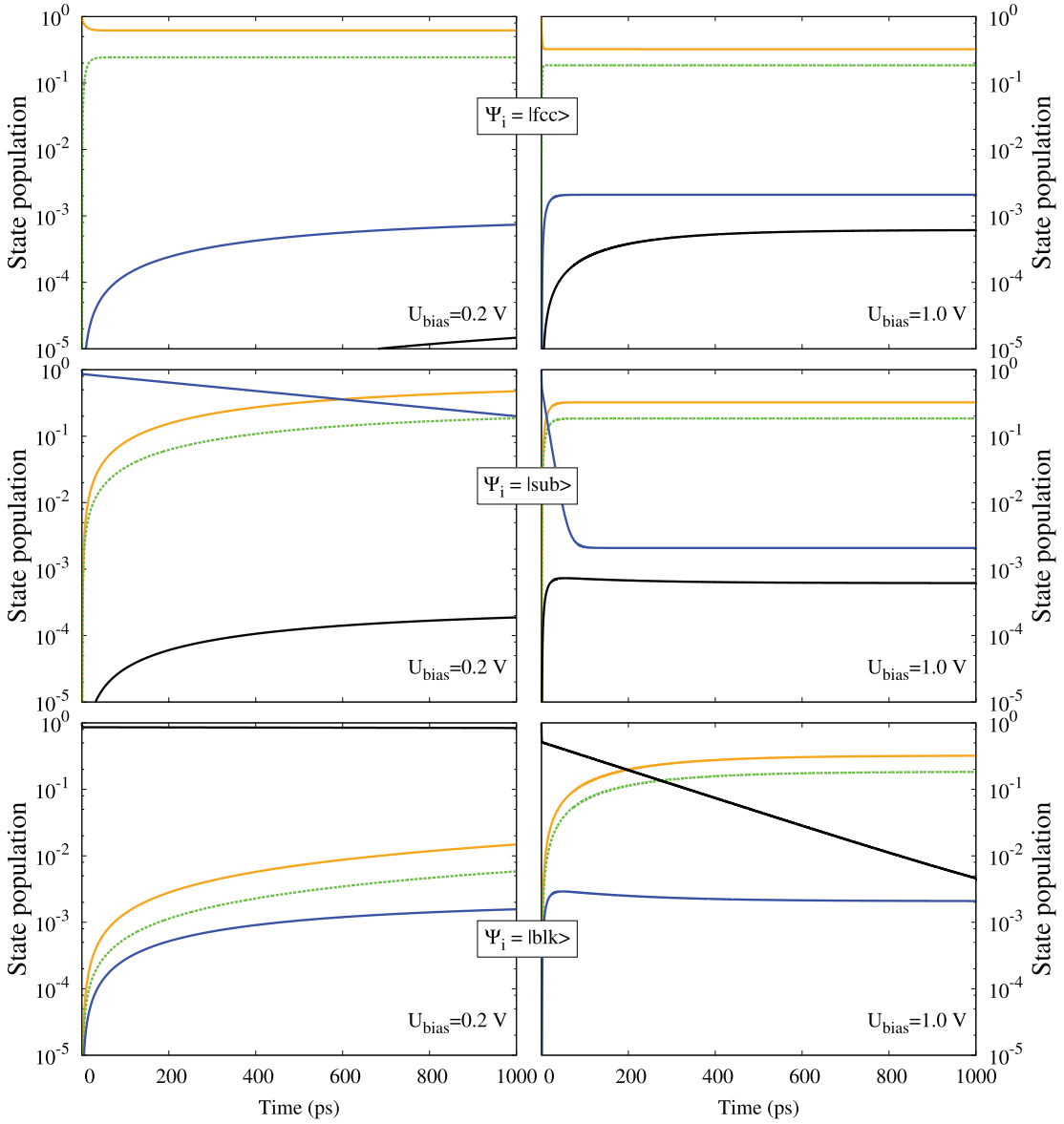

FIG. 5. Population evolution of the fcc (orange), hcp (dashed green), subsurface (blue), and bulk (black) ground states for different initial states at potential bias $U = 0.2$ V (left panels) and $U = 1.0$ V (right panels). (Top panels) Population decay from the fcc ground state. (Central panels) Population decay from the subsurface octahedral site. (Bottom panels) Population decay from the bulk octahedral site.

surface. After turning on the STM, the zeroth-order states become connected by the perturbation and reach a quasi stationary state, which is a subtle interplay between upward and downward rates of all dissipative channels connected pairwise by detailed balance. After switching off the STM, the system is allowed to relax (dashed arrow) and can reach a configuration that is far from the thermal equilibrium, depending on the degree of delocalization inside and outside the surface of the intermediate states reached upon excitation. By varying the potential bias of the STM tip, the dynamics could, in principle, be steered towards desired reaction products. Note that tunneling is included explicitly in the model by using the delocalized bound states as a basis for the dynamics and by explicitly considering the position-dependence and the anharmonicity in the determination of the non-adiabatic coupling rates.

Figure 5 shows the population evolution of the fcc, hcp, octahedral subsurface, and octahedral bulk sites for different initial configurations. The population dynamics for a potential bias of $U = 0.2$ V (left panels) and $U = 1.0$ V (right panels) is shown for an excitation time of 1 ns. Starting with system in its global ground state (top panels), the system is found to equilibrate very rapidly at both potential biases. Most of the population is found in either the fcc or in the hcp ground states at the end of the simulation, with only small residual excitation in the subsurface and the bulk. This can be explained by the small barrier to lateral diffusion (∼1250 hc/cm) compared to the barrier to the subsurface (∼4600 hc/cm). Hence, the population remains trapped at the surface. The potential bias mostly affects the ratio of the hcp to fcc population at the end of propagation and the timescale required to reach a quasi-stationary evolution of the populations. As could be expected,

this effect is even more pronounced for a system initially prepared in the subsurface (central panels) and in the bulk (bottom panels). In the former, the system does not reach a quasi-stationary state at lower bias. This can be rationalized using Eq. (8), where the prefactor $|eU|/\hbar\omega_{ij}$ can be understood as an enhancement factor for the non-adiabatic couplings. At potential bias $U = 0.2$ V, the energy injected by the STM is $|eU| = 1613$ hc/cm, which is about the classical barrier to resurfacing (∼1600 hc/cm from the subsurface minimal geometry). In this case, tunneling dominates the dynamics. For the larger potential bias $U = 1.0$ V, the injected energy is much above the barrier and above-threshold diffusion dominates. Accordingly, the populations reaches a quasi-stationary state much more rapidly (see central right panel of Figure 5).

Interestingly, most of the population is found in the fcc and hcp ground states at the end of the simulations. This is due to the fact that the STM-induced transitions couple all states reversibly and, hence, the system will evolve towards a quasi-thermal equilibrium. Assuming a Boltzmann distribution of the populations in a two-state model, the latter can be characterized by an effective temperature of about $T_{eff} = 443$ K for $U = 0.2$ V and $T_{eff} = 741$ K for $U = 1.0$ V. These temperatures describe a situation far from equilibrium, even after the perturbation is switched off and the system is allowed to cool down. A similar conclusion can be drawn for excitations from the bulk, where the population ratio of the hcp to fcc ground states reach the same effective temperatures, but the dynamics happens on a longer timescale because of the higher bulk-to-subsurface diffusion barrier (∼2650 hc/cm).

Sykes and co-workers[56] have shown experimentally that it is possible to manipulate hydrogen atoms below a palladium surface by using a STM to create islands of subsurface hydrogen atoms. These are identified as protuberances on the flat surface due to the relaxation of the first layer of palladium atoms when the subsurface sites are occupied. The proposed mechanism is that bulk hydrogen diffuse to the subsurface to create these islands. From the simulations presented here, it is clear that the experiment cannot be explained by the pseudo-thermal diffusion of bulk hydrogen to the subsurface due to non-adiabatic coupling. This is in contradiction with the claims by Blanco-Rey *et al.*[53] Note that the distortion of the barrier heights due to the applied bias is not included in their model. One could argue that the relaxation of the palladium lattice is neglected in the present model. It was shown by Kasai and co-workers that this reduces both the bulk-to-subsurface and the resurfacing barriers.[68] As such, this would only favor the resurfacing of bulk hydrogen at the expense of the subsurface population.

Figure 6 shows the population depletion of the three different initial states (orange, blue, and black, respectively) for a bias voltage of $U = 1$ V. On the logarithmic scale, two timescales can be clearly identified during the excitation dynamics. The first population drop happens in the subpicosecond regime and appears to be independent of the initial state. We can rationalize this feature as a response of the system to the STM current, where all states becomes coupled and quickly reach a quasi-equilibrium. At longer times, the population is seen to leak from the initial state towards other sites. Physically, this longer timescale corresponds to the transfer

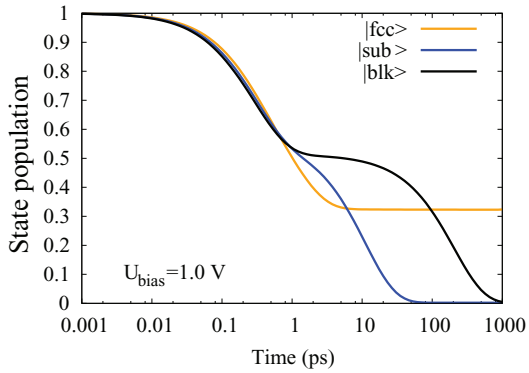

FIG. 6. STM-induced population decay for a fcc (orange), subsurface (blue), and bulk (black) initial states at potential bias $U_{bias} = 1$ V. The initial response of the system to the perturbation happens on a similar timescale in all three cases. A second decay mechanism depending on the initial state can be observed at longer times.

time of the atomic impurity from its initial site. This is the timescale that should be compared to the one reported in experiments. A good estimate is only available for xenon on nickel,[41] where it ranges from 100 μs to about 1 s for potential bias below 1 V. For the two higher initial states (subsurface, blue; bulk, black), the population is quantitatively transferred by the STM perturbation at times longer than 100 ps and 1 ns, respectively. These timescales should be taken carefully because of the uncertainty associated with the determination of the scaling constant w_s, which might change the exact value of the potential bias used in the simulation.

The population decays can be fitted to a double exponential function of the form

$$P_n(t) = 1 + C_r(e^{-t/\tau_r} - 1) + C_t(e^{-t/\tau_t} - 1). \qquad (13)$$

Here, C_r and C_t are interpreted as a response and a transfer efficiency, respectively, with associated rates $1/\tau_r$ and $1/\tau_t$. The top, central, and bottom panels of Table II show the parameters for a system initially prepared in the fcc, subsurface octahedral, or bulk octahedral site, respectively. Response times of about 0.5 ps for all three initial conditions are consistent with the state-resolved lifetimes reported in Sec. III A. This is the time needed by the system to react to the perturbation of its equilibrium state via creation of short-lived electron-hole pairs. In the simulation, the perturbation is switched on abruptly, whereas it would build up very slowly in an STM experiment. A lengthy discussion of the response time thus appears somewhat artificial, but the chosen excitation procedure allows to optimally decouple the system response from the transfer time, which is the physically meaningful quantity.

As expected, the transfer times correlate well with the diffusion barrier of the initial site. Transfer times from the subsurface and bulk sites vary strongly from 683 to 11 ps and from 36.4 ns to 206 ps, respectively. These are well below the experimental upper bound of minutes for the H/Pd(111)[56] and the transfer times for similar systems (e.g., ∼100 μs at 1 V for Xe/Ni[41]). The energy given by the STM at $U = 0.2$ V ($|eU| = 1613$ hc/cm) is small in comparison to the activation barriers (∼1600 and ∼2650 hc/cm, respectively) and tunneling is the dominating mechanism. At higher voltages where above-threshold transfer dominates, the transfer times

TABLE II. Parameters for the population decay of various initial states induced by excitation using a scanning tunneling microscope, as a function of the applied potential bias. The response τ_r and transfer times τ_t obtained from fitting Eq. (13) are reported along with the amplitude of each mechanism. The last column reports the population of the state after a 1 ns excitation time followed by a 5 ps equilibration time. (Top part) Population decay from the fcc ground state. (Central part) Population decay from the subsurface octahedral site. (Bottom part) Population decay from the bulk octahedral site.

U_{bias}	τ_r (ps)	C_r	τ_t (ps)	C_t	P_{1ns}
0.2	0.435	0.110	8.91	0.271	0.715
0.4	0.391	0.186	3.83	0.303	0.679
0.6	0.347	0.237	2.31	0.330	0.657
0.8	0.308	0.269	1.61	0.359	0.641
1.0	0.271	0.286	1.22	0.391	0.629
0.2	0.436	0.140	683	0.854	0.232
0.4	0.398	0.247	115	0.752	0.001
0.6	0.361	0.328	39.4	0.671	0.002
0.8	0.326	0.389	19.0	0.609	0.003
1.0	0.296	0.435	11.0	0.563	0.004
0.2	0.397	0.140	36400	0.820	0.974
0.4	0.371	0.253	5300	0.744	0.829
0.6	0.349	0.346	1340	0.653	0.476
0.8	0.328	0.423	471	0.576	0.121
1.0	0.308	0.487	206	0.513	0.009

diminish significantly but the transition between both regimes appears to be smooth.

Following a relaxation period of 5 ps at 0 K, the population dynamics in the different wells have all reached quasi-stationary states. The initial state population at the end of the cooling cycle is reported in the last column of Table II. Although the temperature is set to zero in all simulations, the system is found far from equilibrium after the equilibration period. This is because part of the molecules have been transferred irreversibly from their initial state. The remaining population in the initial well at the end of the cooling cycle should reach about $P_{1ns} \simeq 1 - C_t$. This rule of thumb is in fair agreement with the results for excitations starting from the fcc center. For the subsurface excitation, this seems only to hold for the lowest bias voltage. At $U = 0.4$ eV, the excitation energy is large enough to overcome the diffusion barrier and the population transfers almost quantitatively from the initial site to both the fcc and hcp sites. The reason is that, once the barrier is overcome, the atomic impurity can delocalize above all available minima, as depicted schematically in Figure 4. As the temperature decreases, the system will then relaxes to the most stable sites more rapidly, and the estimate of the transfer efficiency provided by C_t is lost.

The response and transfer rates, defined as the inverse of the associated times, are depicted, respectively, in the bottom and top panels of Figure 7 as a function of the applied potential bias. From the bottom panel, the response rates from the bulk (black), the subsurface (blue), and fcc (orange) initial states emerge as almost linear in all cases, pointing out at a system-dependent response property. Since the exact rise and fall of the STM excitation are not included properly in the present model, the response time will not be discussed further. It was observed experimentally that STM-induced atom

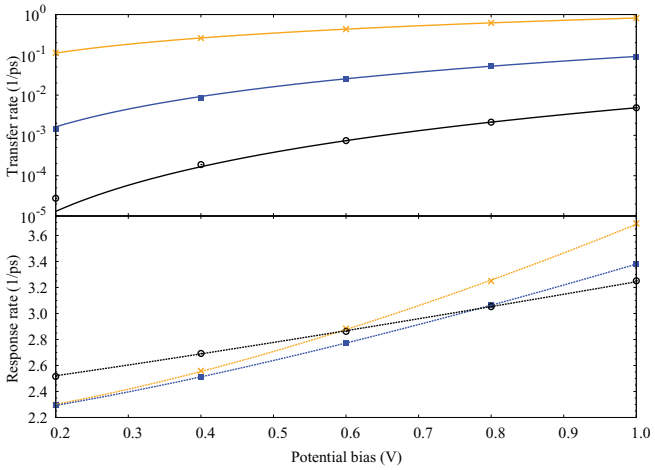

FIG. 7. Response (bottom panel) and transfer rates (top panel) obtained from Eq. (13) for the population decay from a fcc (orange), subsurface (blue), and bulk (black) initial state, as a function of the applied bias potential. The response and transfer rates were fitted to Eq. (14).

transfers follow a power law:[41]

$$\gamma_t \propto U^n. \tag{14}$$

In the limit of a 1D truncated harmonic potential, the exponent n for the transfer rates γ_t can be interpreted as the number of levels below the barrier.[52] Using this formula to fit the curves in Figure 7, one finds $\gamma_t \propto U^{1.245}$, $\gamma_t \propto U^{2.499}$, and $\gamma_t \propto U^{3.678}$ for systems prepared initially in the fcc, subsurface, and bulk sites, respectively. The exponents suggest that about one bound state is localized in the fcc well, whereas about 2.5 would be involved in the transition from the subsurface octahedral site and almost 4 states from the bulk octahedral site. Again, these findings are consistent with the associated barrier heights. For example, in the bulk site, 4 vibrational quanta along the Z-mode (633 hc/cm) bring the hydrogen close to the top of the classical diffusion barrier (2532 hc/cm vs ∼2650 hc/cm).

IV. CONCLUSION

In conclusion, a general model was developed for treating non-adiabatic effects beyond the local harmonic approximation. The derivation based on a source-bridge-sink inelastic electron transfer appears to capture the physics of both energy relaxation and STM-induced transitions equally well. Imposing explicitly the appropriate relations between upward and downward rates in both cases allows to circumvent the limitation of the product ansatz for the vibronic wave functions, while introducing the position dependence of the non-adiabatic couplings in the rate expressions. The relaxation rates are found to depend on the local electron density surrounding the bridge times the gradient along a given vibrational mode. The STM excitations are found to be directly proportional to the relaxation rates, multiplied by an energy transfer factor of the form $|eU|/\hbar\omega$, which grows linearly with the potential bias. The efficiency of the STM-induced transitions depends also linearly on a prefactor, w_s, which can be related to the partial widths of the density of states of the

source and the sink projected on the bridge state. Since these quantities are not well defined, the prefactor should be used as a scaling factor in any realistic simulation and adjusted to reliable experiments.

The model was applied to study the dynamics of a hydrogen impurity at a palladium(111) surface. In all stable adsorption and absorption sites, lifetimes on the order of ∼500 fs were found for the first excited states along the modes parallel and perpendicular to the surface. Proper treatment of vibrational anharmonicity and approximate inclusion of the position-dependence of the non-adiabatic couplings also allowed for electron-mediated intermode coupling and transfer between different sites. For the system at hand, an estimate of the STM-transition efficiency, $w_s \simeq 0.02$, could be obtained from periodic density functional calculations. Excitation times on the order of the 1–100 ps were determined for both modes perpendicular and parallel to the surface on the potential bias range $U = [0, 1]$ V. The lifetime of the latter mode was found to be almost independent of the initial site, whereas the perpendicular mode had a larger spread at different sites that correlate well with the associated diffusion barriers.

The incoherent population dynamics of the system driven by an STM tip was studied using a Pauli master equation. For the system prepared initially in the fcc, subsurface, or bulk sites, the system was found to reach a quasi-equilibrium state at a rate that depends on the potential bias and the diffusion barriers. In all cases, the population was found to decay outside the surface at longer times, consistent with a quasi-thermal behavior for the system under the STM perturbation. This is in apparent contradiction with the hypothesis that subsurface hydrogen atoms can be brought selectively from the bulk to subsurface using a STM. If this is the case, the mechanism does not appear to originate from the non-adiabatic couplings at the palladium surface.

The time evolution of the population of different initial states reveals two timescales for the population loss due to non-adiabatic couplings. A response time on the order of the system lifetimes (∼500 fs) is found to be dependent about linearly on the potential bias and independent of the initial state pointing out at a system dependent property. The other timescale is much longer (from ∼8 ps to ∼36 ns at low voltage, depending on the initial site) and contains the information about the transfer rate induced by STM. This is below the upper limit imposed by experiment. The voltage dependence of the transfer rates is found to obey a power law of the form $\gamma_t \propto U^n$, conform to experimental findings on similar systems. From the fits, the simple interpretation of the exponent n as the number of bound states below the diffusion barrier in a truncated harmonic potential appears to hold.

The transparent derivation of the non-adiabatic coupling rate expressions presented in the Appendix allows to identify elements that could be improved in future work. In particular, the variation of the projected density of states around the Fermi energy should be included. Further, the asymmetry in the STM-induced transitions with respect to the sign of the potential bias could be added using a potential term. Finally, because of the dynamics happen on a long timescales, lattice relaxation should be treated either by recomputing the potential energy surface or by inclusion of vibration-phonon coupling in the rate expression.

ACKNOWLEDGMENTS

The author is indebted to Peter Saalfrank, Iñaki Juaristi, Maite Alducin Ochoa, and María Blanco-Rey for numerous fruitful discussions. The funding of the Deutsche Forschungsgemeinschaft through the Emmy-Noether program (Project No. TR1109/2-1) is acknowledged.

APPENDIX: POSITION-DEPENDENT ANHARMONIC NON-ADIABATIC TRANSITION RATE

1. General considerations

The full Hamiltonian of the system can be written as a sum of electronic $\hat{H}_e$ and vibrational $\hat{H}_v$ contributions,

$$\hat{H} = \hat{H}_e \otimes \hat{I}_v + \hat{I}_e \otimes \hat{H}_v + \hat{H}_{ev}, \tag{A1}$$

where the last term represents the electron-vibration coupling. The coupling between metal electrons and an adsorbate vibrations induces electronic transitions and is mediated by the kinetic energy operator of the nuclei. For a given mode q associated with a mass m_q, we define the coupling Hamiltonian as

$$\hat{H}_{ev} = \frac{-\hbar^2}{2m_q}\frac{\partial^2}{\partial q^2}. \tag{A2}$$

The transition rates are given in first-order perturbation theory by

$$\Gamma^{(q)}_{i\to j} = \frac{2\pi}{\hbar}\sum_{\alpha\beta}|\langle\alpha, j|\hat{H}_{ev}|\beta, i\rangle|^2 f_\beta(E_\beta)(1 - f_\alpha(E_\alpha)) \times \delta(E_\alpha - E_\beta - \hbar\omega_{ij}), \tag{A3}$$

where ω_{ij} is the transition frequency between vibrational states $|i\rangle$ and $|j\rangle$, and $f_{\alpha,\beta}$ are Fermi distributions for the initial and final electronic states. The delta-function ensures energy conservation. Factorizing the vibronic wave functions, $|\alpha, j\rangle = |\alpha\rangle|j\rangle$, expanding the operator in the basis, and neglecting second-order terms of the form $\langle\alpha|\frac{\partial^2}{\partial q^2}|\beta\rangle$, we get

$$\Gamma^{(q)}_{i\to j} = \frac{2\pi\hbar^3}{m_q^2}\sum_{\alpha\beta}\left|\langle j|\langle\alpha|\frac{\partial}{\partial q}|\beta\rangle\frac{\partial}{\partial q}|i\rangle\right|^2 f_\beta(E_\beta)\,(1 - f_\alpha(E_\alpha)) \times \delta(E_\alpha - E_\beta - \hbar\omega_{ij}). \tag{A4}$$

It is known that

$$\langle\alpha|\frac{\partial}{\partial q}|\beta\rangle = \frac{\langle\alpha|\frac{\partial\hat{H}_e}{\partial q}|\beta\rangle}{(E_\beta - E_\alpha)}, \tag{A5}$$

where E_α (E_β) is the energy of electronic state $|\alpha\rangle$ ($|\beta\rangle$). By energy conservation, the electronic energy difference is equal to the transition frequency $(E_\beta - E_\alpha) = \hbar\omega_{ij}$. Substituting in

Eq. (A4), we get

$$\Gamma^{(q)}_{i\to j} = \frac{2\pi\hbar}{m_q^2\omega_{ij}^2}\sum_{\alpha\beta}\left|\langle j|\langle\alpha|\frac{\partial\hat{H}_e}{\partial q}|\beta\rangle\frac{\partial}{\partial q}|i\rangle\right|^2 \times f_\beta(E_\beta)(1-f_\alpha(E_\alpha))\,\delta(E_\alpha - E_\beta - \hbar\omega_{ij}). \quad \text{(A6)}$$

According to Gao, Persson, and Lundqvist,[52] the nonadiabatic couplings are dominated by a single resonance located on the adsorbate, $|a\rangle$. The state $|a\rangle$ can be more generally interpreted as a bridge linking a source and a sink density of states. Let us define the projectors,

$$\hat{P}_a + \hat{Q}_a = 1, \text{ where } \hat{P}_a = |a\rangle\langle a| \text{ and } \hat{Q}_a = 1 - \hat{P}_a. \quad \text{(A7)}$$

The electronic contribution can be written as

$$\langle\alpha|\frac{\partial\hat{H}_e}{\partial q}|\beta\rangle = \langle\alpha|\hat{P}_a\frac{\partial\hat{H}_e}{\partial q}\hat{P}_a|\beta\rangle + \langle\alpha|\hat{P}_a\frac{\partial\hat{H}_e}{\partial q}\hat{Q}_a|\beta\rangle + \langle\alpha|\hat{Q}_a\frac{\partial\hat{H}_e}{\partial q}\hat{P}_a|\beta\rangle + \langle\alpha|\hat{Q}_a\frac{\partial\hat{H}_e}{\partial q}\hat{Q}_a|\beta\rangle. \quad \text{(A8)}$$

The projection on $\hat{P}_a$ is thought to dominate the coupling and the projection on $\hat{Q}_a$ is neglected altogether. The electronic contribution now reads

$$\langle\alpha|\frac{\partial\hat{H}_e}{\partial q}|\beta\rangle \simeq \langle\alpha|a\rangle\langle a|\frac{\partial\hat{H}_e}{\partial q}|a\rangle\langle a|\beta\rangle. \quad \text{(A9)}$$

The electronic expectation value that appears in the equation could be simplified according to the Hellmann-Feynman theorem as $\varepsilon'_a(\vec{R}) = \langle a|\frac{\partial\hat{H}_e}{\partial q}|a\rangle$ in the case where $|a\rangle$ is an eigenstate of $\hat{H}_e$. This must not be the case but we choose this definition to simplify notation. The generalization is straightforward. After substitution in Eq. (A6), we find

$$\Gamma^{(q)}_{i\to j} \simeq \frac{2\pi\hbar}{m_q^2\omega_{ij}^2}\sum_{\alpha\beta}\left|\langle j|\varepsilon'_a\langle\alpha|a\rangle\langle a|\beta\rangle\frac{\partial}{\partial q}|i\rangle\right|^2 \times f_\beta(E_\beta)(1-f_\alpha(E_\alpha))\,\delta(E_\alpha - E_\beta - \hbar\omega_{ij}). \quad \text{(A10)}$$

Let us now discuss the terms appearing in Eq. (A10):

- $\varepsilon'_a(\vec{R})$ is the variation of the bridge state energy with respect to the nuclear coordinates, which is a function of the adsorbate position $\vec{R}$ at the surface. It is often stated that this term is well approximated by the variation of the adsorbate affinity level, embedded in a jellium of variable density. From preliminary calculations, this does not seem to be the case. It is thus preferable to keep ε'_a as a scaling parameter to be defined later.
- $\langle\alpha|a\rangle$ is a source term depending on the shape of the multi-electron wave function and the position $\vec{R}$ of the bridge state.
- $\langle a|\beta\rangle$ is a sink term depending on the shape of the multi-electron wave function and the position $\vec{R}$ of the bridge state.

Now, let us introduce a complete continuous pointwise representation for the nuclear coordinates, $1 = \int d\vec{R}_\nu|\vec{R}_\nu\rangle\langle\vec{R}_\nu|$, on the right of the electronic terms:

$$\Gamma^{(q)}_{i\to j} \simeq \frac{2\pi\hbar}{m_q^2\omega_{ij}^2}\sum_{\alpha\beta}\left|\langle j|\langle\alpha|a\rangle\langle a|\beta\rangle\varepsilon'_a(\vec{R})\int d\vec{R}_\nu|\vec{R}_\nu\rangle\langle\vec{R}_\nu|\frac{\partial}{\partial q}|i\rangle\right|^2 \times f_\beta(E_\beta)(1-f_\alpha(E_\alpha))\,\delta(E_\alpha - E_\beta - \hbar\omega_{ij})),$$
$$\Gamma^{(q)}_{i\to j} \simeq \frac{2\pi\hbar}{m_q^2\omega_{ij}^2}\sum_{\alpha\beta}\left|\int d\vec{R}_\nu\langle j|\vec{R}_\nu\rangle\langle\alpha|a(\vec{R}_\nu)\rangle\langle a(\vec{R}_\nu)|\beta\rangle\varepsilon'_a(\vec{R}_\nu)\langle\vec{R}_\nu|\frac{\partial}{\partial q}|i\rangle\right|^2 \times f_\beta(E_\beta)(1-f_\alpha(E_\alpha))\,\delta(E_\alpha - E_\beta - \hbar\omega_{ij})). \quad \text{(A11)}$$

Expanding the quadratic expression and rearranging the terms, we get

$$\Gamma^{(q)}_{i\to j} \simeq \frac{2\pi\hbar}{m_q^2\omega_{ij}^2}\sum_{\alpha\beta}\left\{\int d\vec{R}_\nu\langle j|\vec{R}_\nu\rangle\langle\alpha|a(\vec{R}_\nu)\rangle\langle a(\vec{R}_\nu)|\beta\rangle\varepsilon'_a(\vec{R}_\nu)\langle\vec{R}_\nu|\frac{\partial}{\partial q}|i\rangle\right\} \times\left\{\int d\vec{R}_\mu\langle i|\frac{\partial}{\partial q}|\vec{R}_\mu\rangle\langle\beta|a(\vec{R}_\mu)\rangle\langle a(\vec{R}_\mu)|\alpha\rangle\varepsilon'_a(\vec{R}_\mu)\langle\vec{R}_\mu|j\rangle\right\} \times f_\beta(E_\beta)(1-f_\alpha(E_\alpha))\,\delta(E_\alpha - E_\beta - \hbar\omega_{ij})),$$
$$\Gamma^{(q)}_{i\to j} \simeq \frac{2\pi\hbar}{m_q^2\omega_{ij}^2}\sum_{\alpha\beta}\int d\vec{R}_\nu\int d\vec{R}_\mu\left\{\langle j|\vec{R}_\nu\rangle\langle\beta|a(\vec{R}_\nu)\rangle\langle a(\vec{R}_\mu)|\beta\rangle\varepsilon'_a(\vec{R}_\nu)\langle\vec{R}_\nu|\frac{\partial}{\partial q}|i\rangle\right\} \times\left\{\langle i|\frac{\partial}{\partial q}|\vec{R}_\mu\rangle\langle\alpha|a(\vec{R}_\mu)\rangle\langle a(\vec{R}_\nu)|\alpha\rangle\varepsilon'_a(\vec{R}_\mu)\langle\vec{R}_\mu|j\rangle\right\} \times f_\beta(E_\beta)(1-f_\alpha(E_\alpha))\,\delta(E_\alpha - E_\beta - \hbar\omega_{ij})). \quad \text{(A12)}$$

Neglecting the two-point correlation of the source, $\langle\beta|a(\vec{R}_\mu)\rangle\langle a(\vec{R}_\nu)|\beta\rangle \rightarrow (\langle\beta|a(\vec{R}_\nu)\rangle\langle a(\vec{R}_\nu)|\beta\rangle)$, and sink terms, $\langle\alpha|a(\vec{R}_\nu)\rangle\langle a(\vec{R}_\mu)|\alpha\rangle \rightarrow (\langle\alpha|a(\vec{R}_\mu)\rangle\langle a(\vec{R}_\mu)|\alpha\rangle)$, it is possible to separate both the summations over α, β, and the integrals in Eq. (A12):

$$\Gamma^{(q)}_{i\rightarrow j} \simeq \frac{2\pi\hbar}{m_q^2\omega_{ij}^2}\left\{\int d\vec{R}_\nu\langle j|\vec{R}_\nu\rangle\left(\sum_\beta\langle\beta|a(\vec{R}_\nu)\rangle\langle(\vec{R}_\nu)a|\beta\rangle\right)\varepsilon_a'(\vec{R}_\nu)\langle\vec{R}_\nu|\frac{\partial}{\partial q}|i\rangle\right\}$$
$$\times\left\{\int d\vec{R}_\mu\langle i|\frac{\partial}{\partial q}|\vec{R}_j\rangle\left(\sum_\alpha\langle\alpha|a(\vec{R}_\mu)\rangle\langle a(\vec{R}_\mu)|\alpha\rangle\right)\varepsilon_a'(\vec{R}_\mu)\langle\vec{R}_\mu|j\rangle\right\}$$
$$\times f_\beta(E_\beta)\,(1-f_\alpha(E_\alpha))\,\delta(E_\alpha-E_\beta-\hbar\omega_{ij})\Big). \tag{A13}$$

The separation yields an equation reminiscent of Bardeen theory and unique expressions are recovered for appropriate choices for the density of states (see below).

The density of source and sink states at a given configuration $\vec{R}_\nu$, $\vec{R}_\mu$ are, respectively,

$$\sum_\beta\langle\beta|a(\vec{R}_\mu)\rangle\langle a(\vec{R}_\mu)|\beta\rangle = \int_{-\infty}^{\epsilon_F} dE_\beta\rho^{source}_{\vec{R}_\mu}(E_\beta),$$
$$\sum_\alpha\langle\alpha|a(\vec{R}_\nu)\rangle\langle a(\vec{R}_\nu)|\alpha\rangle = \int_{\epsilon_F-eU}^{\infty} dE_\alpha\rho^{sink}_{\vec{R}_\nu}(E_\alpha), \tag{A14}$$

where U is a potential bias and ϵ_F is the source Fermi energy. From Eq. (A13), we then get

$$\Gamma^{(q)}_{i\rightarrow j} \simeq \frac{2\pi\hbar}{m_q^2\omega_{ij}^2}\left\{\int d\vec{R}_\nu\langle j|\vec{R}_\nu\rangle\int_{-\infty}^{\epsilon_F} dE_\beta\rho^{source}_{\vec{R}_\mu}(E_\beta)\varepsilon_a'(\vec{R}_\nu)\langle\vec{R}_\nu|\frac{\partial}{\partial q}|i\rangle\right\}$$
$$\times\left\{\int d\vec{R}_\mu\langle i|\frac{\partial}{\partial q}|\vec{R}_\mu\rangle\int_{\epsilon_F-eU}^{\infty} dE_\alpha\rho^{sink}_{\vec{R}_\nu}(E_\alpha\varepsilon_a'(\vec{R}_\mu)\langle\vec{R}_\mu|j\rangle\right\}$$
$$\times f_\beta(E_\beta)\,(1-f_\alpha(E_\alpha))\,\delta(E_\alpha-E_\beta-\hbar\omega_{ij})). \tag{A15}$$

Note that all electronic coordinates are now integrated out and consequently vanish from Eq. (A13). A change of variable, $\epsilon = \epsilon_F - E_\beta$, allows to further resolve one of the energy integrals using the Dirac δ-function and define the new integration boundaries:

$$\Gamma^{(q)}_{i\rightarrow j} \simeq \frac{2\pi\hbar}{m_q^2\omega_{ij}^2}\int_0^{\hbar\omega_{ij}+eU} d\epsilon\left\{\int d\vec{R}_\nu\langle j|\vec{R}_\nu\rangle\varepsilon_a'(\vec{R}_\nu)\rho^{source}_{\vec{R}_\nu}(\epsilon_F-\epsilon)\langle\vec{R}_\nu|\frac{\partial}{\partial q}|i\rangle\right\}$$
$$\times\left\{\int d\vec{R}_\mu\langle i|\frac{\partial}{\partial q}|\vec{R}_\mu\rangle\varepsilon_a'(\vec{R}_\mu)\rho^{sink}_{\vec{R}_\mu}(\epsilon_F-\epsilon+\hbar\omega_{ij})\langle\vec{R}_\mu|j\rangle\right\}$$
$$\times f_\beta(\epsilon_F-\epsilon)(1-f_\alpha(\epsilon_F-\epsilon+\hbar\omega_{ij})). \tag{A16}$$

The terms in parenthesis can be interpreted as a transfer of momentum between the electrons, $\varepsilon_a'(\vec{R}_k)$, and the nuclei, $\langle\vec{R}_k|\frac{\partial}{\partial q}|i\rangle$, averaged on the position of the nuclei, $\int d\vec{R}_k$, and weighted by the nuclear wave function, $\langle j|\vec{R}_k\rangle$, and the electronic projected density of states, $\rho_{\vec{R}_k}$, at any given nuclear configuration. To avoid the non-local form of the non-adiabatic coupling expression (A16), the equation is rewritten as

$$\Gamma^{(q)}_{i\rightarrow j} \simeq \frac{2\pi\hbar}{m_q^2\omega_{ij}^2}\int_0^{\hbar\omega_{ij}+eU} d\epsilon\left\{\langle j|\varepsilon_a'(\vec{R})\rho^{source}_{\vec{R}}(\epsilon_F-\epsilon)\frac{\partial}{\partial q}|i\rangle\right\}$$
$$\times\left\{\langle i|\frac{\partial}{\partial q}\varepsilon_a'(\vec{R})\rho^{sink}_{\vec{R}}(\epsilon_F-\epsilon+\hbar\omega_{ij})|j\rangle\right\}f_\beta(\epsilon_F-\epsilon)(1-f_\alpha(\epsilon_F-\epsilon+\hbar\omega_{ij})). \tag{A17}$$

Provided the density of states is almost constant on the energy range of interest,[52] the rate expression can be further simplified as

$$\Gamma^{(q)}_{i\to j} \simeq \frac{2\pi\hbar}{m_q^2\omega_{ij}^2}\left\{\langle j|\varepsilon_a'(\vec{R})\rho_{\vec{R}}^{source}(\epsilon_F)\frac{\partial}{\partial q}|i\rangle\right\}\left\{\langle i|\frac{\partial}{\partial q}\varepsilon_a'(\vec{R})\rho_{\vec{R}}^{sink}(\epsilon_F)|j\rangle\right\} \times \int_0^{\hbar\omega_{ij}+eU} d\epsilon f_\beta(\epsilon_F-\epsilon)(1-f_\alpha(\epsilon_F-\epsilon+\hbar\omega_{ij})). \quad \text{(A18)}$$

This is a general equation that can be applied to compute any relaxation rate due to non-adiabatic coupling. Specific modeling for the density of states is required to get expressions for the relaxation rates and the STM-induced rates.

Since the choice of the source or sink densities of state at a given position could be interchanged, the following identity should hold

$$\langle j|\varepsilon_a'(\vec{R})\rho_{\vec{R}}^{source}(\epsilon_F)\frac{\partial}{\partial q}|i\rangle\langle i|\frac{\partial}{\partial q}\varepsilon_a'(\vec{R})\rho_{\vec{R}}^{sink}(\epsilon_F)|j\rangle = \langle j|\varepsilon_a'(\vec{R})\rho_{\vec{R}}^{sink}(\epsilon_F)\frac{\partial}{\partial q}|i\rangle\langle i|\frac{\partial}{\partial q}\varepsilon_a'(\vec{R})\rho_{\vec{R}}^{source}(\epsilon_F)|j\rangle \quad \text{(A19)}$$

in Eq. (A18). This amounts to neglecting the commutator error for the operators $\frac{\partial}{\partial q}$ and $\varepsilon_a'(\vec{R})\rho_{\vec{R}}(\epsilon_F)$. This approximation is strictly valid only if the last operator is independent of the position, which is a direct consequence of the choice of a factorizable form for the vibronic wave functions in Eq. (A4). The commutator error will remain small provided the electronic contribution to the non-adiabatic couplings is small and varies smoothly with the adsorbate position. These are also the conditions of validity for the perturbative treatment of non-adiabatic couplings. By using the left-hand side of Eq. (A19) to compute the rates in Eq. (A18) and enforcing explicitly the proper relation between upward and downward transition rates, we have a simple way of overcoming the physical limitation imposed by the product ansatz for the wave function in Eq. (A4) while avoiding the commutator error.

2. Zero-bias relaxation

In the absence of an STM tip (i.e., $U = 0$), both source and sink densities of states are equal to the projected density of states on the adsorbate bridge, $\rho^{sink}(\epsilon_F) = \rho^{source}(\epsilon_F) = \rho(\epsilon_F)$, and Eq. (3) simplifies as

$${}^{\rm eh}\Gamma^{(q)}_{i\to j} \simeq \frac{2\pi\hbar}{m_q^2\omega_{ij}^2}\left|\langle j|\varepsilon_a'\rho(\epsilon_F)\frac{\partial}{\partial q}|i\rangle\right|^2\int_0^{\hbar\omega_{ij}} d\epsilon f_\beta(\epsilon_F-\epsilon) \times (1-f_\alpha(\epsilon_F-\epsilon+\hbar\omega_{ij})). \quad \text{(A20)}$$

The superscript *eh* is used to emphasize that the underlying mechanism is the coupling of the vibrations to electron-hole pairs of the metal substrate. The latter can serve both as a source and a sink for the electrons. In the absence of an STM tip, this is the only coupling mechanism considered in the model. Following Gao and co-workers, the integral over the Fermi functions is replaced by a Bose-Einstein distribution, $B(\hbar\omega_{nm})$,

$$\int_0^{\hbar\omega_{ij}} d\epsilon f_\beta(\epsilon_F-\epsilon)(1-f_\alpha(\epsilon_F-\epsilon+\hbar\omega_{ij})) \simeq \hbar\omega_{ij}(1+B(\hbar\omega_{ij})). \quad \text{(A21)}$$

This is not necessary but renders the result more elegant while enforcing detailed balance on the converse rate. The expression thus becomes

$${}^{\rm eh}\Gamma^{(q)}_{i\to j} \simeq \frac{2\pi\hbar^2}{m_q^2\omega_{ij}}\left|\langle j|\varepsilon_a'\rho(\epsilon_F)\frac{\partial}{\partial q}|i\rangle\right|^2(1+B(\hbar\omega_{ij})). \quad \text{(A22)}$$

The main goal of this work is to find a physically sound approximation for the variation of the function $\varepsilon_a'\rho(\epsilon_F)$ as a function of the adsorbate position, while still properly treating anharmonic effects by resolving the integral in Eq. (A22) numerically.

To mimic the position-dependence of the non-adiabatic couplings, let us now assume that the adsorbate is embedded in a locally spherical jellium of density $\mathbf{n}$, which depends on the position and shape of the impurity. The Wigner-Seitz radius r_s of the local free electron gas depends on the electron density of the environment at any given position. This approximation should be valid in the limit of an infinitesimally small volume V. The density of states in a three-dimensional free electron gas of volume $V = 4\pi r_s^3/3 = N_e/\mathbf{n}$ at energy $\epsilon_F = \hbar^2k_f^2/2m_e$ and Fermi momentum $k_f = (3\pi^2\mathbf{n})^{1/3}$ is known analytically,

$$\rho(\epsilon_F) = \left(\frac{3^{1/3}N_em_e}{\pi^{4/3}\hbar^2}\right)\mathbf{n}^{-2/3}, \quad \text{(A23)}$$

where m_e is the electron mass. This choice is consistent with a point-wise representation for the local projected density of states $\rho(\epsilon_F)$. The rate expression (A22) then takes the form

$${}^{\rm eh}\Gamma^{(q)}_{i\to j} \simeq \left(\frac{72^{1/3}N_e^2}{\pi^{5/3}}\right)\left(\frac{m_e^2}{\hbar^2m_q^2\omega_{ij}}\right)\left|\langle j|\frac{\varepsilon_a'}{\mathbf{n}^{2/3}}\frac{\partial}{\partial q}|i\rangle\right|^2 \times (1+B(\hbar\omega_{ij})). \quad \text{(A24)}$$

In previous work,[38,39] we demonstrated that, for an atomic impurity in a locally spherical electron gas, the electronic part of the non-adiabatic coupling elements varies as $\mathbf{n}^{1/3}$. To recover the same position-dependence, the derivative of the bridge state energy with respect to the nuclear coordinate must follow the electron density,

$$\varepsilon_a' = \left(\frac{\varepsilon_a'}{\mathbf{n}}\right)\Big|_{\rm ref}\cdot\mathbf{n}, \quad \text{(A25)}$$

where the scaling factor $(\frac{\varepsilon'_a}{\mathbf{n}})|_{\text{ref}}$ is a constant evaluated at a reference position. The model thus simplifies to our previous model with a different definition for the scaling constant:

$$
\begin{aligned}
{}^{\text{eh}}\Gamma^{(q)}_{i\to j} &\simeq \frac{\gamma^{(q)}}{\omega_{ij}} \left|\langle j|\mathbf{n}^{1/3}\frac{\partial}{\partial q}|i\rangle\right|^2 (1+B(\hbar\omega_{ij}));\gamma^{(q)} \\
&= \left(\frac{72^{1/3}N_e^2m_e^2}{\pi^{5/3}\hbar^2m_q^2}\right)\left(\frac{\varepsilon'_a}{\mathbf{n}}\right)\Bigg|^2_{\text{ref}}. \qquad \text{(A26)}
\end{aligned}
$$

Here, the energy-dependence of the transition rates due to electron-hole pair coupling is taken into account explicitly and found to be inversely proportional to the transition energy. Upwards transition rates are obtained from the same matrix elements as

$$
\Gamma^{(q)}_{i\leftarrow j} \simeq \frac{\gamma^{(q)}}{\omega_{ij}} \left|\langle j|\mathbf{n}^{1/3}\frac{\partial}{\partial q}|i\rangle\right|^2 B(\hbar\omega_{ij}), \qquad \text{(A27)}
$$

since $1+B(\hbar\omega_{ji}) = 1+B(-\hbar\omega_{ij}) = B(\hbar\omega_{ij})$. The rates obey detailed balance.

The calculation of the bridge state energy shift ε'_a can prove quite cumbersome. The main feature of the model is that it proposes a systematic treatment of both the anharmonicity of the vibrations and the position-dependence of non-adiabatic coupling for all states. The relation among the state-resolved anharmonic rates should thus be valid up to a scaling constant, which depends on the subtle balance of electronic effects in the metal-adsorbate system. In a practical implementation of Eqs. (A26) and (A27), it is preferable to define the scaling constant using a reference geometry that is known to be strongly localized and harmonic, e.g., the global minimum of the potential energy surface. The scaling constant $\gamma^{(q)}$ can then be obtained by comparison to the local harmonic limit of Eq. (A26):

$$
\gamma^{(q)} = \left(\frac{2\hbar\Gamma^{(ref,q)}}{m_q\mathbf{n}^{2/3}_{(ref)}}\right). \qquad \text{(A28)}
$$

The reference embedding density, $\mathbf{n}_{(ref)}$, is defined as a locally spherical free electron gas with the Wigner-Seitz radius r_s of the free metal density evaluated at the reference position.

3. STM-induced transition

At finite bias, the integral over the Fermi functions in Eq. (A18) can be simplified as[52]

$$
\int_0^{\hbar\omega_{ij}+eU} d\epsilon f_\beta(\epsilon_F-\epsilon)(1-f_\alpha(\epsilon_F-\epsilon+\hbar\omega_{ij})) \simeq |eU|. \qquad \text{(A29)}
$$

This should be valid for $|eU| \gg \hbar\omega_{ij}$ leading to an error which increases linearly. From Eq. (A18), it can be seen that the rates scale quadratically with $1/\omega_{ij}$. The linear error should thus not affect the results significantly. By changing the integration boundaries and the Fermi distributions in Eq. (A18) to take into account the reverse process where the electrons flow from the substrate to the tip ($U<0$), Eq. (A29) is found independent of the sign of the potential bias.

For the STM-to-metal transfer, the sink density of states is replaced by that of a locally spherical jellium with a parabolic dispersion, Eq. (A23), where the electron density $\mathbf{n}$ is that of the metallic environment. As shown above, the position-dependence of the bridge state energy shift is proportional to the electron density, that is, the total electron density. Since the substrate contribution to the total electron density is much larger than that of the STM, the former can be used in the equation. Note that the energetic position of the adsorbate bridge state depends on the applied bias, $\varepsilon_a \to \varepsilon_a(U(\vec{R}))$, but this is neglected here:

$$
\begin{aligned}
{}^{\text{stm}}\Gamma^{(q)}_{i\to j} &\simeq \left(\frac{24^{1/3}N_em_e|eU|}{\pi^{1/3}m_q^2\hbar\omega_{ij}^2}\right)\left(\frac{\varepsilon'_a}{\mathbf{n}}\right)\Bigg|^2_{\text{ref}} \\
&\quad\times \langle j|\mathbf{n}\rho^{source}(\epsilon_F)\frac{\partial}{\partial q}|i\rangle\langle i|\frac{\partial}{\partial q}\mathbf{n}^{1/3}|j\rangle. \qquad \text{(A30)}
\end{aligned}
$$

To find the position-dependence of the source term for the STM $\to$ bridge $\to$ metal transfer, the partial density of states $\rho^{source}(\epsilon_F)$ is again replaced by a locally spherical jellium density:

$$
\rho^{source}(\epsilon_F) = \left(\frac{3^{1/3}N_em_e}{\pi^{4/3}\hbar^2}\right)\mathbf{n}^{-2/3}_{source}. \qquad \text{(A31)}
$$

The source electron density can be represented roughly using an embedding atom model:

$$
\mathbf{n}_{source} \propto \mathbf{n}_{\text{EAM}} = \mathbf{n}_{\text{W}}(|\vec{q}-\vec{Q}_{\text{tip}}|) + \sum_{\mu=1}^{N_s}\mathbf{n}_\mu(|\vec{q}-\vec{Q}_\mu|). \qquad \text{(A32)}
$$

Here, $\mathbf{n}_\mu$ is the electron density at position $\vec{q}$ due to substrate atom μ located at position $\vec{Q}_\mu$, and $\mathbf{n}_{\text{W}}$ is the electron density of a single tip atom (usually tungsten). The choice of spherically symmetric jellium is consistent with the recent finding that STM-induced transitions in the bulk are induced by s-wave propagation of the electrons in the metal.[53]

Recognizing that $\mathbf{n}_{\text{W}} \to 0$ everywhere but in close vicinity of the tip, this implies that, to a good approximation, potential contributions from other orbitals of the STM tip during the injection process can be neglected. The electron density of the tip is thus proportional to the electron density of the metallic environment:

$$
\rho^{source}(\epsilon_F) = \left(\frac{3^{1/3}N_em_e}{\pi^{4/3}\hbar^2}\right)\mathbf{n}^{-2/3}_{source} \simeq \left(\frac{3^{1/3}N_em_e}{\pi^{4/3}\hbar^2}\right)\frac{w_s}{\mathbf{n}^{2/3}}. \qquad \text{(A33)}
$$

The factor w_s is a scaling factor proportional to the s-projected density of states.

According to test calculations on the H/Pd(111) system, the ratio of the s-projected density of states to the total density of states at the Fermi energy remains almost constant for both the free metal and in the presence of an atomic impurity. The parameter w_s can thus be considered constant, yielding the following rate equation:

$$
{}^{\text{stm}}\Gamma^{(q)}_{i\to j} \simeq w_s\left(\frac{|eU|}{\hbar\omega_{ij}}\right)\left(\frac{\gamma^{(q)}}{\omega_{ij}}\right)\left|\langle j|\mathbf{n}^{1/3}\frac{\partial}{\partial q}|i\rangle\right|^2, \qquad \text{(A34)}
$$

where $\gamma^{(q)}$ is the same as for the relaxation rates, Eq. (4).

[1]U. Fano, Phys. Rev. **124**, 1866 (1961).
[2]D. C. Langreth, Phys. Rev. Lett. **54**, 126 (1985).
[3]H. Conrad, M. E. Kordesch, W. Stenzel, and M. Sunjic, J. Vac. Sci. Technol. A **5**, 452 (1987).
[4]P. Dumas, M. Suhren, Y. J. Chabal, C. J. Hirschmugl, and G. P. Williams, Surf. Sci. **371**, 200 (1997).
[5]A. R. P. Rau, Phys. Scr. **69**, C10 (2004).
[6]H. Conrad, R. Scala, W. Stenzel, and R. Unwin, J. Chem. Phys. **81**, 6371 (1984).
[7]A. D. Johnson, K. J. Maynard, S. P. Daley, Q. Y. Yang, and S. T. Ceyer, Phys. Rev. Lett. **67**, 927 (1991).
[8]J. Strömquist, L. Bengtsson, M. Persson, and B. Hammer, Surf. Sci. **397**, 382 (1998).
[9]S. Wright, J. F. Skelly, and A. Hodgson, Chem. Phys. Lett. **364**, 522 (2002).
[10]J. R. Trail, M. Graham, D. M. Bird, M. Persson, and S. Holloway, Phys. Rev. Lett. **88**, 166802 (2002).
[11]H. Winter, J. I. Juaristi, I. Nagy, A. Arnau, and P. M. Echenique, Phys. Rev. B **67**, 245401 (2003).
[12]T. Mitsui, M. K. Rose, E. Fomin, D. F. Ogletree, and M. Salmeron, Nature (London) **422**, 705 (2003).
[13]A. C. Luntz and M. Persson, J. Chem. Phys. **123**, 074704 (2005).
[14]M. S. Mizielinski, D. M. Bird, M. Persson, and S. Holloway, J. Chem. Phys. **122**, 084710 (2005).
[15]A. C. Luntz, M. Persson, S. Wagner, C. Frischkorn, and M. Wolf, J. Chem. Phys. **124**, 244702 (2006).
[16]P. Nieto, E. Pijper, D. Barredo, G. Laurent, R. A. Olsen, E.-J. Baerends, G.-J. Kroes, and D. Far'as, Science **312**, 86 (2006).
[17]J. I. Juaristi, M. Alducin, R. Díez Muiño, H. F. Busnengo, and A. Salin, Phys. Rev. Lett. **100**, 116102 (2008).
[18]D. M. Bird, M. S. Mizielinskia, M. Lindenblattb, and E. Pehlkeb, Surf. Sci. **602**, 1212 (2008).
[19]M. Timmer and P. Kratzer, Phys. Rev. B **79**, 165407 (2009).
[20]M. Richter, A. Carmele, S. Butscher, N. Bücking, F. Milde, P. Kratzer, M. Scheffler, and A. Knorr, J. Appl. Phys. **105**, 122409 (2009).
[21]G.-J. Kroes, C. Diaz, E. Pijper, R. A. Olsen, and D. J. Auerbach, Proc. Natl. Acad. Sci. U.S.A. **107**, 20881 (2010).
[22]A. C. Luntz, M. Persson, and G. O. Sitz, J. Chem. Phys. **124**, 091101 (2006).
[23]A. M. Wodtke, D. Matsiev, and D. J. Auerbach, Prog. Surf. Sci. **83**, 167 (2008).
[24]J. Kröger, J. Phys.: Condens. Matter **20**, 224015 (2008).
[25]A. Nourtier, J. Phys. (France) **38**, 479 (1977).
[26]R. Festa and E. G. d'Agliano, Physica A **90**, 229 (1978).
[27]K. Schönhammer and O. Gunnarsson, Z. Phys. B: Condens. Matter **38**, 127 (1980).
[28]M. Persson and B. Hellsing, Phys. Rev. Lett. **49**, 662 (1982).
[29]K. Schönhammer and O. Gunnarsson, Phys. Rev. B **27**, 5113 (1983).
[30]M. J. Puska and R. M. Nieminen, Phys. Rev. B **27**, 6121 (1983).
[31]B. Hellsing and M. Persson, Phys. Scr. **29**, 360 (1984).
[32]T. T. Rantala and A. Rosén, Phys. Rev. B **34**, 837 (1986).
[33]K. Schönhammer, O. Gunnarsson, and L. Bönig, Prog. Surf. Sci. **26**, 1 (1987).
[34]M. Head-Gordon and J. C. Tully, J. Chem. Phys. **96**, 3939 (1992).
[35]J. C. Tully, M. Gomez, and M. Head-Gordon, J. Vac. Sci. Technol. A **11**, 1914 (1993).
[36]D. Fuhrmann and C. Wöll, New J. Phys. **1**, 1 (1998).
[37]V. Krishna and J. C. Tully, J. Chem. Phys. **125**, 054706 (2006).
[38]J. C. Tremblay and P. Saalfrank, J. Chem. Phys. **131**, 084716 (2009).
[39]J. C. Tremblay, S. Monturet, and P. Saalfrank, Phys. Rev. B **81**, 125408 (2010).
[40]J. C. Tremblay, S. Monturet, and P. Saalfrank, J. Phys. Chem. A **115**, 10698 (2011).
[41]D. M. Eigler, C. P. Lutz, and W. E. Rudge, Nature (London) **352**, 600 (1991).
[42]J. Bardeen, Phys. Rev. Lett. **6**, 57 (1961).
[43]J. Tersoff and D. R. Hamann, Phys. Rev. B **31**, 805 (1985).
[44]B. N. J. Persson and A. Baratoff, Phys. Rev. Lett. **59**, 339 (1987).
[45]N. Lorente and M. Persson, Faraday Discuss. **117**, 277 (2000).
[46]N. Lorente and M. Persson, Phys. Rev. Lett. **85**, 2997 (2000).
[47]R. Walkup, D. M. Newns, and P. Avouris, J. Electron Spectrosc. Relat. Phenom. **64**, 523 (1993).
[48]R. Walkup, D. M. Newns, and P. Avouris, Phys. Rev. B **48**, 1858 (1993).
[49]S. Gao, M. Persson, and I. Lundqvist, Solid State Commun. **84**, 271 (1992).
[50]S. Gao, M. Persson, and I. Lundqvist, J. Electron Spectrosc. Relat. Phenom. **64**, 665 (1993).
[51]S. Gao, Phys. Rev. B **55**, 1876 (1997).
[52]S. Gao, M. Persson, and I. Lundqvist, Phys. Rev. B **55**, 4825 (1997).
[53]M. Blanco-Rey, M. Alducin, J. I. Juaristi, and P. de Andres, Phys. Rev. Lett. **108**, 115902 (2012).
[54]J. M. Blanco, F. Flores, and R. Pérez, Prog. Surf. Sci. **81**, 403 (2006).
[55]Here, the notation **n** is preferred to ρ_{embd} to avoid confusion with the projected density of states.
[56]E. C. H. Sykes, L. C. Fernández-Torres, S. U. Nanayakkara, B. A. Mantooth, R. M. Nevin, and P. S. Weiss, Proc. Natl. Acad. Sci. U.S.A. **102**, 17907 (2005).
[57]H. OuYang, B. Källbering, and R. Marcus, J. Chem. Phys. **98**, 7565 (1993).
[58]K. Zenichowski, T. Klamroth, and P. Saalfrank, Appl. Phys. A **93**, 319 (2008).
[59]B. N. J. Persson and J. E. Demuth, Solid State Commun. **57**, 769 (1986).
[60]N. Ozawa, T. A. Roman, H. Nakanishi, H. Kasai, N. B. Arboleda, Jr., and W. A. Diño, J. Appl. Phys. **101**, 123530 (2007).
[61]Y. J. Chabal, Phys. Rev. Lett. **55**, 845 (1985).
[62]J. E. Reutt, Y. J. Chabal, and S. B. Christman, Phys. Rev. B **38**, 3112 (1988).
[63]J. Kröger, S. Lehwand, and H. Ibach, Phys. Rev. B **55**, 10895 (1997).
[64]The pseudopotentials "Pd.pbe-nd-rrkjus.UPF" and "H.pbe-rrkjus.UPF" from http://www.quantum-espresso.org are used for palladium and hydrogen, respectively.
[65]J. P. Perdew, K. Burke, and M. Ernzerhof, Phys. Rev. Lett. **78**, 1396 (1997).
[66]P. Giannozzi, S. Baroni, N. Bonini, M. Calandra, R. Car, C. Cavazzoni, D. Ceresoli, G. L. Chiarotti, M. Cococcioni, I. Dabo, A. D. Corso, S. Fabris, G. Fratesi, S. de Gironcoli, R. Gebauer, U. Gerstmann, C. Gougoussis, A. Kokalj, M. Lazzeri, L. Martin-Samos, N. Marzari, F. Mauri, R. Mazzarello, S. Paolini, A. Pasquarello, L. Paulatto, C. Sbraccia, S. Scandolo, G. Sclauzero, A. P. Seitsonen, A. Smogunov, P. Umari, and R. M. Wentzcovitch, J. Phys.: Condens. Matter **21**, 395502 (2009).
[67]H. J. Monkhorst and J. D. Pack, Phys. Rev. B **13**, 5188 (1976).
[68]K. Nobuhara, H. Nakanishi, H. Kasai, and A. Okiji, J. Appl. Phys. **88**, 6897 (2000).